Simulation of the spatiotemporal aspects of land erodibility in the northeast Lake Eyre Basin, Australia, 1980–2006

Nicholas P. Webb,[1,2] Hamish A. McGowan,[2,3] Stuart R. Phinn,[1] Grant H. McTainsh,[2,4] and John F. Leys[2,5]

[1]   This paper explores spatiotemporal patterns in land erodibility in the northeast portion of the Lake Eyre Basin, Australia, using the Australian Land Erodibility Model (AUSLEM) in simulations from 1980 to 2006. First, spatial patterns in land erodibility are examined. We then present an analysis of seasonal and interannual variations in land erodibility. Patterns in land erodibility change are compared to rainfall variability, the El Niño–Southern Oscillation (ENSO) and Pacific (inter-) Decadal Oscillation (PDO). Land erodibility is found to peak in the study area between early spring (September, October, November) and late summer (January, February, March), and reach a minimum over winter (June, July, August). Weak correlations are found between modeled land erodibility, rainfall, ENSO, and the PDO. The results indicate a complex landscape response to climate variability, with land erodibility dynamics being affected by antecedent rainfall and vegetation conditions which generate lag responses in land erodibility change. The research highlights the importance of developing methods for monitoring conditions driving variations in wind erosion at the landscape scale to enhance land management policy in arid and semiarid landscapes at a time of uncertain future climate changes.

1. Introduction

[2]   Wind erosion and mineral dust emissions play important roles in land surface and atmospheric processes at local (<1 km^2) to global scales [*Miller and Tegen*, 1998; *Lal*, 2001; *Jickells et al.*, 2005]. While dust emission and transport mechanisms have received much attention, the spatial extent of dust source areas and conditions driving temporal variations in land erodibility remain poorly understood [*McTainsh et al.*, 1999; *Mahowald et al.*, 2003a]. Analyses of atmospheric dust concentrations indicate that land erodibility is a dynamic condition that is highly variable through space and time [*Brooks and Legrand*, 2000]. Spatial and temporal variations in land erodibility at the landscape scale (10^3 km^2) are important controls on

regional-scale (10^4 km^2) dust transport [*Gillette*, 1999]. Numerous modeling systems have been developed to assess wind erosion dynamics at regional to global scales, e.g., DPM [*Marticorena and Bergametti*, 1995], DEAD [*Zender et al.*, 2003a], GOCART [*Ginoux et al.*, 2004], and in Australia models have successfully been applied to simulate dust emissions within the Lake Eyre and Murray-Darling river basins [*Shao and Leslie*, 1997; *Lu and Shao*, 2001; *Shao et al.*, 2007]. However, there remains a significant lack of research into the application of these models to assess land erodibility dynamics at the landscape scale.

[3]   Mapping and monitoring land susceptibility to wind erosion is required to enhance land management to combat land degradation and desertification of dryland environments [*Oldeman*, 1994; *Sivakumar*, 2007]. Quantifying rates of anthropogenic (accelerated) and naturally occurring wind erosion is a fundamental component of this work. This is dependent on an understanding of factors driving variations in dust emissions at the landscape scale [*Mahowald et al.*, 2003b]. Modeling spatial and temporal patterns in land erodibility can be used to establish baseline levels of variability in the landscape response to climate and land management conditions. The effects of climate and land management changes on potential erosion can then be assessed with knowledge of the likely response of landscapes to these external drivers. Increasing pressures on natural resource use in rangelands [*Galvin et al.*, 2008], and increasing aridity and rainfall variability in the subtropics

[1]Centre for Remote Sensing and Spatial Information Science, School of Geography, Planning and Architecture, University of Queensland St. Lucia, Brisbane, Queensland, Australia.

[2]Also at Desert Knowledge Cooperative Research Centre, Alice Springs, Northern Territory, Australia.

[3]School of Geography, Planning and Architecture, University of Queensland St. Lucia, Brisbane, Queensland, Australia.

[4]Australian Rivers Institute, Faculty of Environmental Sciences, Griffith University, Brisbane, Queensland, Australia.

[5]Scientific Services Division, Department of Environment and Climate Change, Gunnedah, New South Wales, Australia.
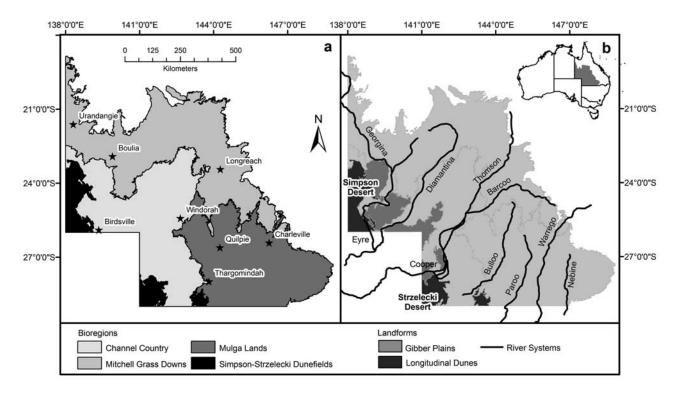
Figure 1. Study area map showing the study area location: (a) bioregions and townships, and (b) major river systems and significant landforms, including dune fields and gibber (stony) plains.

[*Hu and Fu*, 2007; *Meehl et al.*, 2007] make understanding these land surface-climate-management dynamics essential for the sustainable use of the world's drylands.

[4] A number of techniques have been employed to determine the location and extent of areas susceptible to wind erosion. *Prospero et al.* [2002] and *Washington et al.* [2003] used aerosol optical thickness data from the Total Ozone Mapping Spectrometer (TOMS) to characterize persistent global dust source areas. The studies demonstrated an association of source areas with internally draining river systems and topographic depressions. Modeling dust source areas using topographic erodibility indicators was subsequently employed by *Ginoux et al.* [2001] and *Zender et al.* [2003b] in a comparison of dust emission simulations using geomorphic and hydrological erodibility factors. The application of surface reflectance factors derived from Moderate Resolution Imaging Spectroradiometer (MODIS) data to define erodible land areas has also been investigated [*Grini et al.*, 2005]. Limitations to these approaches have been their coarse spatial resolution (typically ∼1° lat./long.) and inability to detect local temporal variations in source strength (land erodibility). Furthermore, unless satellite images are selected to coincide with dust emission events [e.g., *Bullard et al.*, 2008] the accuracy of this method for detecting dust source locations is affected by the fact that satellites capture transported dust that may not be overlying active source areas. Because of this, care must be taken when using the data for model calibration and validation, which are dependent on accurate source area identification.

[5] At the regional scale (10^4 km^2), maps of areas affected by wind erosion tend to be interpretive and based on climatic indicators (e.g., aridity), or on the frequency at which dust storms are recorded over a particular area [e.g.,

McTainsh et al., 1989, 1990]. Similarly, temporal changes in land erodibility have been inferred from seasonal and annual trends in observed dust storm frequencies [*Goudie and Middleton*, 1992; *McTainsh et al.*, 1998]. The detail of spatial and temporal variations in land erodibility is therefore very coarse, as vast distances (>100 km) often separate stations recording dust events in arid and semiarid areas [*McTainsh and Leys*, 1993]. The growing availability of remote sensing products and model simulations of land surface conditions, e.g., vegetation cover and soil moisture, presents the opportunity to map and monitor land erodibility dynamics at moderate to high resolutions (<10^3 m^2, daily – monthly), and address the lack of research in this area.

[6] This research seeks to quantify patterns in land erodibility dynamics in the northeastern portion of the Lake Eyre Basin, Australia; arguably the largest dust source in the Southern Hemisphere [*Goudie and Middleton*, 2006]. The aim of this paper is to analyze simulations from the Australian Land Erodibility Model (AUSLEM) [*Webb et al.*, 2009] (1) to identify spatial patterns in land erodibility in the northern sector of the Lake Eyre Basin, western Queensland; (2) to identify the frequency at which areas are susceptible to wind erosion in this region; and (3) to identify temporal patterns in land erodibility, with a focus on documenting mechanisms driving seasonal and interannual variations in land erodibility dynamics.

2. Study Area

[7] The study area is the arid and semiarid rangelands located in the north and northeast of the Lake Eyre Basin in western Queensland (Figure 1). The area receives 200–500 mm a^{-1} rainfall and maximum air temperatures range

from >40°C in summer (December, January, February, DJF) to the high teens and middle twenties in winter (June, July, August, JJA). The study area is ~672 000 km^2 in size and can be divided into four biogeographical regions, herein bioregions (DEWR, 2007, http://www.environment.gov.au/parks/nrs/science/bioregion-framework/ibra/index.html). These include (1) Channel Country, forb fields and grassland downs with intervening anabranching river systems and woodlands, and small areas of sand plains and dunes in the floodplain sediments; (2) Mitchell Grass Downs, undulating downs (grasslands) and low woodlands on gray and brown cracking clay soils; (3) Mulga Lands, shrublands and low woodlands on undulating plains and low hills on red earths and lithosols; and (4) Simpson-Strzelecki Dune fields, arid dune fields and sand plains with sparse shrublands and hummock grasslands. Salt lakes and playas are dispersed among the dunes. Rivers dissect the region and their channels are fringed with narrow woodlands.

[8] The boundary of the semiarid zone, along the 450–500 mm rainfall isohyet, borders the eastern boundaries of the Mulga Lands and Mitchell Grass Downs. Wind erosion is infrequently observed outside this zone due to higher annual rainfall and vegetation cover, so that area is not considered here. Land use in the study area is dominated by pastoral agriculture with sheep and cattle grazing of rangelands.

3. Model Description

3.1. Model Framework and Input Data

[9] Land susceptibility to wind erosion, i.e., land erodibility, was modeled with the Australian Land Erodibility Model (AUSLEM). The model was developed by *Webb et al.* [2009] as a Geographic Information System (GIS) tool, and builds on a rule-based modeling scheme presented by *Webb et al.* [2006]. The model is run at a 5 × 5 km spatial resolution on a daily time step. AUSLEM predicts land erodibility by integrating subroutines that account for soil texture, soil moisture, vegetation and surficial stone cover effects on the susceptibility of the land surface to wind erosion.

[10] The model subroutines are based on empirical functions selected to capture the physical nature of the land erodibility continuum. That is, the range of erodibility conditions that a land area may experience for a given range of soil erodibility and surface roughness conditions [*Webb et al.*, 2009]. AUSLEM is different from other wind erosion models in that it: 1) operates at the landscape scale (10^3 km^2) on a daily time step; and 2) does not seek to quantify erosion rates or dust emissions. Rather, AUSLEM makes specific assessments of land erodibility which are modeled on a continuous and dimensionless scale (from 0 not erodible to 1 highly erodible). The model subroutines are integrated through a multiplicative approach [after *Shao*, 2000] in the form

$$E_r = E_{tx}(tx)E_{gc}(gc)E_w(w)E_{tc}(tc)E_{rk}(rk) \qquad (1)$$

where E_r is the land erodibility (0 to 1). $E_{gc}(gc)$ and $E_w(w)$ define the relationships between grass cover, soil water content and land erodibility. These continuous functions allow for the effects of grass cover and soil water to be modeled through the full range of the erodibility continuum.

$E_{gc}(gc)$ defines the negative exponential relationship between land erodibility and percentage grass cover (%gc):

$$E_{gc} = \alpha \exp^{-\beta^{(\%gc)}} \qquad (2)$$

where α and β are regression coefficients (55.873; −0.0938) denoting the equation intercept and rate of change in erodibility given a change in percentage cover [after *Leys*, 1991]. The relationship follows the form of those identified by *Fryrear* [1985], *Findlater et al.* [1990], and *Lyles and Allison* [1981] for prostrate and standing cover, respectively.

[11] Soil water effects on land erodibility are modeled through a relationship between soil water conditions and the frequency of local dust events (WMO SYNOP WW 07) observed in the western Queensland study area [*Webb et al.*, 2009]:

$$E_w = \exp^{-\beta^w} \qquad (3)$$

where β is a regression coefficient (−0.236) denoting the sensitivity of local dust event frequencies to source area soil water content. While the expression relates soil water content to local dust event frequencies, it has a form similar to that identified by *Shao et al.* [1996] and is the only expression suitable for application with the available soil moisture input data [*Webb et al.*, 2009]. The dimensionless scaling of AUSLEM allows for the grass cover and soil moisture schemes to be calibrated without violating assumptions inherent to models utilizing parameterizations of the threshold friction velocity (u_{*t}) for particle entrainment (another measure of erodibility).

[12] The $E_{tc}(tc)$ and $E_{rk}(rk)$ components are thresholds to account for the effects of shrub/tree cover and surficial stone cover. The E_{tc} threshold is applied through a mask that assigns land erodibility values of 0 (not erodible) to areas with shrub/tree cover greater than 20% [after *Marshall*, 1972]. A mask for areas with dense surficial stone cover E_{rk} was derived from aerial photograph assessments (1:250,000 scale) of the extent of stony pavements (gibber) within the study area and were sourced from the Western Arid Regions Land Use Study [*Queensland Department of Primary Industries (QDPI)*, 1974].

[13] In the absence of robust models to predict temporal changes in soil erodibility, soil textural effects, $E_{tx}(tx)$, were considered static [after *Lu and Shao*, 2001] at time scales less than one month. In doing this the output analysis was restricted to scales >10^3 km^2 at which the input conditions were found to best model land erodibility [*Webb et al.*, 2009].

[14] The model grass cover (%) and soil water (mm per top 10 cm of profile) inputs are sourced from the Aussie GRASS pasture growth model [*Carter et al.*, 1996; *Littleboy and McKeon*, 1997]. Calibration and validation of Aussie GRASS was carried out in the Queensland rangelands through comparisons with roadside assessments of pasture condition and time series of vegetation indices (e.g., the normalized difference vegetation index, NDVI) acquired from satellite data [*Carter et al.*, 1996; *Hassett et al.*, 2000]. The grass cover and soil water outputs are most accurate over areas 25–50 times its 5 × 5 km pixel resolution and so

AUSLEM is also likely to perform best at these scales. The implications of this are that validation of AUSLEM and analyses of the model output must be restricted to broad ($>10^3$ km^2) spatial scales. The authors recognize that inaccuracies in the dynamic inputs will affect comparisons of the model output with independent measures of climate variability as explored in this paper.

[15] In the current simulations foliage projective cover (FPC, a vertical projection of tree canopy cover) data for 2003 were used as a representative measure of tree cover. FPC data derived from Landsat ETM+ satellite imagery at a 30×30 m spatial resolution were sourced from the Statewide Landcover and Trees Study [*Danaher et al.*, 2004]. Multitemporal tree cover data can be included in the model simulations when it becomes available.

3.2. Model Performance

[16] AUSLEM performance has been assessed using methods to examine the accuracy of spatiotemporal patterns in the model output. *Webb et al.* [2009] assessed AUSLEM performance through a comparison of output time series with observational records of wind erosion activity. The validation was conducted at four spatial length scales (from 25–150 km) over an 11 year simulation period (1980–1990). Time series model outputs were positively correlated ($r^2 > 0.67$, $p < 0.05$) with trends in dust storm and local dust event (WMO SYNOP WW 07, 09, 30–35) frequencies at six out of eight validation sites [*Webb et al.*, 2009]. AUSLEM is able to capture variations in wind erosion activity, indicative of land erodibility and independent of wind speed variations, in the southern, central and western regions of the study area. The model appears to be least effective in regions with heterogeneous woody vegetation cover to the east of the study area, in the Mulga Lands. The validation was found to be highly dependent on the data representativeness of local wind erosion activity around the sites. At sites to the east of the study area records of wind erosion activity were dominated by dust hazes with nonlocal source areas. These did not provide a fair test of model accuracy and so the poor match in the data at the sites could not specifically be attributed to poor model performance.

[17] Subsequent validation of spatial patterns in the model output (N. P. Webb et al., Validation of the Australian Land Erodibility Model, submitted to *Journal of Arid Environments*, 2008) has confirmed improved model performance in the Channel Country bioregion over the Mulga Lands. The absence of a robust scheme to compute temporal variations in soil erodibility limits AUSLEM performance at spatial scales $<10^3$ km^2, and we note that this issue affects all wind erosion models that lack dynamic soil erodibility schemes [*Lu and Shao*, 2001]. To circumvent this limitation analyses of AUSLEM output are restricted to the landscape to regional scales and monthly to annual temporal resolutions at which soil moisture and surface roughness conditions are adequate predictors of land erodibility [*Webb et al.*, 2009].

4. Model Simulation and Analysis Methods

4.1. Spatial Patterns

[18] AUSLEM was run to assess land erodibility on a daily time step from January 1980 to December 2006. Output was then aggregated into monthly and annual

means. Patterns in the distribution of erodible land were examined by assessing the frequency at which model output was recorded in four land erodibility classes. Arbitrary class boundaries were defined for land that was highly erodible (1–0.15); moderately erodible (0.15–0.0375); had low erodibility (0.0375–0.0091); and was not erodible (0.0091–0). The class boundaries were necessarily nonlinear to account for the exponential increase in land erodibility with decreasing vegetation cover and soil moisture. Mean monthly model output was classified into the four erodibility groups, and the percentage of years (out of 27) in which land occurred in each class was computed on a per pixel basis.

4.2. Seasonal Variability

[19] Seasonal variations in land erodibility were examined by analysis of point time series data. Mean monthly model output values were extracted from areas with 50 km radius around meteorological stations at Birdsville, Boulia, Charleville, Longreach, Thargomindah, Quilpie, Urandangie and Windorah (Figure 1a). Summary statistics of the time series data were computed to provide information on mean monthly land erodibility conditions and the ranges of monthly variations. Trajectories of change in land erodibility within the four study area bioregions (Figure 1a) were then examined by computing the proportional abundance (percentage cover) of each land erodibility class within the bioregions. The analysis was conducted at an annual time scale to provide an indicator of the response of the bioregions to interannual climate variability.

4.3. Interannual Variability

[20] The effects of drought on wind erosion activity have been examined from observational data on atmospheric aerosol concentrations and dust storm frequencies in Africa, the Middle East, North America, China and Australia [*McTainsh et al.*, 1989; *Goudie and Middleton*, 1992; *Brooks and Legrand*, 2000; *Okin and Reheis*, 2002; *Prospero and Lamb*, 2003; *Zender and Kwon*, 2005]. Advances in modeling dust emissions at the global scale have enabled links to be established between atmospheric dust concentrations and climate forcing mechanisms at multiple temporal scales, including the North Atlantic Oscillation (NAO), El Niño–Southern Oscillation (ENSO), Pacific (inter-) Decadal Oscillation (PDO), and others [*Moulin et al.*, 1997; *Mahowald et al.*, 2003b; *Ginoux et al.*, 2004; *Hara et al.*, 2006]. At regional scales the effects of these global teleconnections may be manifested through changes in precipitation and windiness, and have been shown to influence the onset, intensity and duration of drought and periods of enhanced rainfall [e.g., *Allan*, 1988]. It is feasible to hypothesize that land erodibility in western Queensland will also be dynamic and respond to regional to global-scale climate variability.

[21] *Pittock* [1975] demonstrated that annual rainfall is correlated ($r^2 = \sim 0.4$) with the Troup Southern Oscillation Index (SOI) over eastern Australia (east of 138° longitude). The correlation between rainfall and the SOI varies seasonally, and is influenced by phase interactions of ENSO (3–7 year cycle) with the PDO (15–30 year cycle) [*McBride and Nicholls*, 1983; *Power et al.*, 1999; *Crimp and Day*, 2003]. Consequently, episodes of pasture degradation and recovery are linked to variations in Australian rainfall
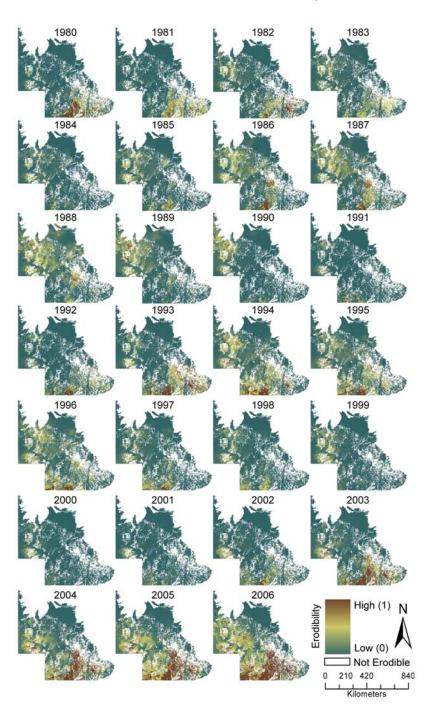
Figure 2. Mean annual land erodibility predictions from AUSLEM for the period 1980 to 2006. White areas are not erodible due to tree and stone cover being above the model threshold.

driven by ENSO-PDO interactions [*McKeon et al.*, 2004]. The final phase of the model output analysis sought to quantify the relationships between dynamic changes in land erodibility, rainfall over western Queensland, and these teleconnections.

[22] A cross-correlation analysis was used to investigate the presence and strength of relationships between mean annual land erodibility and annual total rainfall averaged across the four study area bioregions, and two indicators of the condition of ENSO and the PDO. The Troup Southern

Oscillation Index (SOI) was used in the analysis as a measure of ENSO fluctuations. The Troup SOI data were obtained from the Australian Government Bureau of Meteorology (available at http://www.bom.gov.au/climate/current/soihtm1.shtml) and represent the standardized anomaly of the mean sea level pressure difference between Tahiti and Darwin [*Troup*, 1965]. Monthly PDO index data (available at http://jisao.washington.edu/pdo/PDO.latest) were used to define PDO phases and represent the first principal component of monthly sea surface temperature variability in the
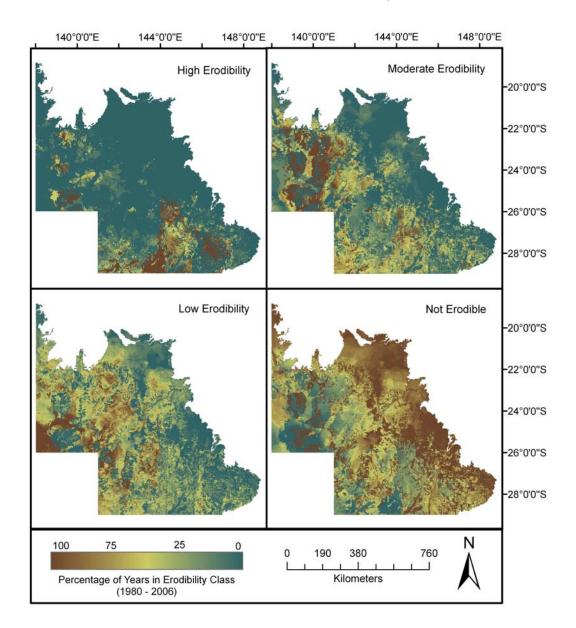
Figure 3. Maps showing the percentage of years in the period 1980 to 2006 in which land in the study area was modeled as having high, moderate, low, and no susceptibility to wind erosion.

North Pacific Ocean [*Mantua et al.*, 1997]. All data were converted to annual averages for the correlation analysis.

5. Results

[23] Figure 2 presents mean annual land erodibility assessments for western Queensland from 1980 to 2006. The following sections analyze patterns in mean monthly model output and the data presented in Figure 2. First, spatial patterns in land erodibility are described. Temporal patterns in land erodibility dynamics are then resolved at seasonal and interannual time scales.

5.1. Spatial Patterns in Land Erodibility

[24] Figure 3 summarizes spatial patterns in land erodibility in western Queensland. Three regions have consistently high land erodibility. These include the Mulga Lands,

Strzelecki Desert, and western side of the Channel Country (refer to Figure 1). In the Mulga Lands high-erodibility land occurs in the mulga (*Acacia aneura*) plains east of the Bulloo River between Quilpie and Thargomindah (Figure 1b). This region extends into the flood-out country and dune fields to the south of the Bulloo River, and across into the Strzelecki Desert dune fields. A third region of high-erodibility land lies between Birdsville and Urandangie along the outer floodplains of the Georgina and Diamantina Rivers. The climates of the areas with consistently high land erodibility are similar. These areas receive <300 mm mean annual rainfall and experience annual evaporation in excess of 2400 mm (Bureau of Meteorology, 2007, http://www.bom. gov.au/climate/index.shtml). The conditions result in a moisture deficiency and sparse vegetation cover that is highly sensitive to grazing pressures [*McKeon et al.*, 2004].
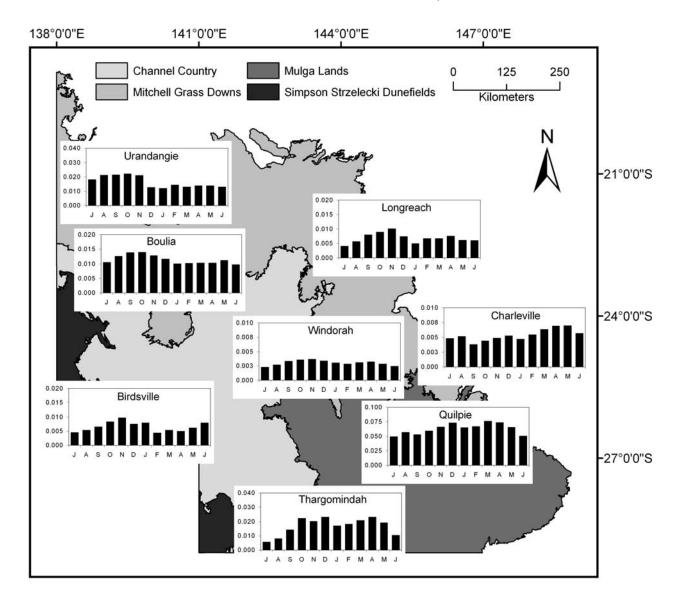
Figure 4. Graphs of mean monthly land erodibility for eight stations across the study area. Data based on daily land erodibility assessments (1980–2006) modeled as a function of vegetation cover and soil attributes and computed as areal means within windows of 50 km radius around the stations.

[25] Areas that frequently have a moderate land erodibility ranking extend from the high-erodibility regions. These areas expand across the driest parts of the study area, covering the western and southern portions of the Channel Country, the Strzelecki dune fields and the western half of the Mulga Lands. A belt of moderately erodible land frequently extends northeast from the Channel Country into the Mitchell Grass Downs near Longreach (see Figure 1b).

[26] Land areas with consistently low and no erodibility occur across the northern and eastern boundaries of the Mitchell Grass Downs and Mulga Lands (Figure 2). This is consistent with the regions receiving on average the highest annual rainfall across the study area [McTainsh and Leys, 1993]. The Channel Country frequently has an elevated land erodibility ranking. Areas that consistently have no erodibility include the gibber plains (stony country) and inner floodplains of the Cooper, Diamantina and Georgina river

systems. The undulating plains between Coopers Creek and the Bulloo River had a low erodibility for much of the period between 1980 and 2006 (Figure 2). This is interesting as surrounding regions generally had higher erodibility rankings. In the southeastern corner of the study area the mulga plains around Charleville generally have a low susceptibility to wind erosion (Figure 3). Extensive surficial stone cover (gibbers) and high tree cover levels reduces the erodibility of these areas. The model identified the Simpson Desert bioregion as having consistently low land erodibility.

5.2. Temporal Dynamics in Land Erodibility

5.2.1. Seasonal Variations

[27] Figure 4 presents graphs of mean monthly land erodibility for eight meteorological stations in western Queensland. Land erodibility has weak seasonality. The strength of seasonal variations changes across the study
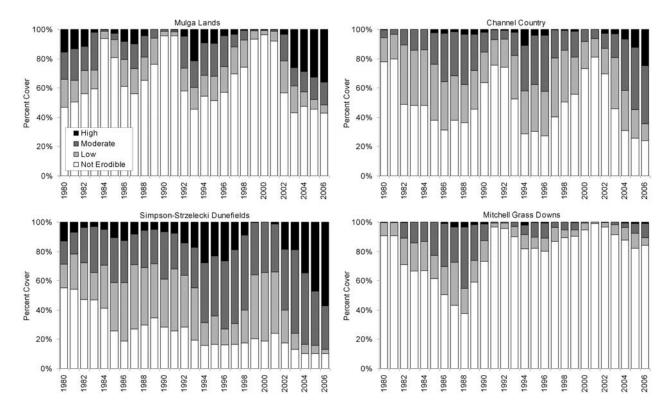
Figure 5. Graphs of annual proportional abundance (percentage cover) of land in the four study area bioregions classified into four land erodibility groups: high, moderate, low, and not erodible.

area and between land types. The largest seasonal variations occur at Quilpie (range 0.027), Thargomindah (range 0.018) and Urandangie (range 0.01). The smallest variations occur at Boulia (range 0.004), Charleville (range 0.003) and Windorah (range 0.001).

[28] There is a north-south spatial pattern in the seasonality of land erodibility across western Queensland (Figure 4). Land erodibility reaches a maximum in spring (September, October, November, SON) and early summer (November, December, ND) in the Channel Country and Mitchell Grass Downs, and a minimum in late summer (January, February, March, JFM) through to winter (JJA). In the Mulga Lands to the south of the study area land erodibility peaks in spring (September, October, November, SON) and autumn (March, April, May, MAM), and reaches a minimum over winter (JJA). These dynamics are consistent with seasonal patterns in dust storm frequencies reported in observational data [Ekström et al., 2004]. The northern pattern reflects a dominance of summer rainfall associated with thunderstorm activity, and a reduction in grass cover through winter and spring associated with lower rainfall. The southern pattern reflects a tendency of the Mulga Lands to receive a less pronounced peak in rainfall over summer and a response to higher winter rainfall [McTainsh et al., 1998].

5.2.2. Interannual Variability

[29] Regional changes in erodible land (Figure 2), and weak seasonal variability (Figure 4) suggest that land erodibility dynamics in western Queensland are driven by forcing mechanisms operating at longer (than monthly) time scales. Figure 5 shows the annual percentage area of each

bioregion covered by land with modeled high, moderate, low and no susceptibility to wind erosion.

[30] Land erodibility dynamics differ markedly between the four bioregions. In the Mulga Lands, land erodibility displays cyclic behavior, with alternating periods of high and low susceptibility to wind erosion. In years of reduced erodibility (e.g., 1984, 1990–1991, 1999–2001) the Mulga Lands appear to "shut down" in terms of the area assessed as being susceptible to wind erosion, with >90% of the bioregion indicated as being not erodible.

[31] In the Channel Country, peaks in land erodibility occurred in similar periods to the Mulga Lands. For every year in the period 1980–2006, >20% of the bioregion had at least a low to moderate susceptibility to wind erosion. In no years did the model indicate a near-complete (>90%) reduction in land erodibility. This consistently erodible condition is a result of the aridity of the bioregion and its inherently low vegetation cover levels.

[32] Land erodibility in the Mitchell Grass Downs was generally low for the analysis period. Temporal changes in land erodibility in this bioregion are distinct in comparison with the other regions. While peaks in erodible land occur at similar times to those in the Channel Country the magnitudes of the peaks are not consistent. The portion of the Mitchell Grass Downs modeled as not being susceptible to wind erosion did not drop below 75% between 1993 and 2006.

[33] Extensive areas (>40%) of the Simpson-Strzelecki bioregion had some susceptibility to wind erosion in each year from 1980 to 2006. This high fractional cover is a

Table 1. Correlation r^2 Between Mean Annual Rainfall, Troup SOI, PDO, and Modeled Land Erodibility for the Four Study Area Bioregions, Based on the 27 Year Simulation[a]

Bioregion	Rainfall	SOI	PDO
Channel Country	−0.19	−0.05	0.28
Mitchell Grass Downs	−0.23	0.09	0.36
Mulga lands	**−0.48**	−0.38	**0.56**
Simpson-Strzelecki Dune fields	−0.09	0.02	−0.16

[a]Significant correlations ($P < 0.05$) are bold.

result of the Strzelecki Desert frequently having elevated land erodibility. The Simpson Desert dune fields did not experience regular high-magnitude changes in erodibility between 1980 and 2006 (Figure 2). These dynamics are evident in the Strezelcki Desert and are indicative of higher grazing pressures, vegetation characteristics (dune fields populated with short-lived grasses (*Aristidia* spp.) and forbs rather than drought-resistant hummock grasses (*Triodia* spp.)), and the higher sensitivity of the region to climate variability.

5.2.3. Land Erodibility, Climate Oscillations, and Rainfall

[34] Table 1 summarizes the correlations between annual rainfall, the SOI, PDO and modeled erodible land cover. There is a negative correlation between rainfall and land erodibility ($r^2 = -0.48$, $p < 0.05$) in the Mulga Lands. This was to be expected given the model's dependence on soil moisture conditions. The relationship weakens in the Mitchell Grass Downs and Channel Country, and is very weak in the Simpson-Strzelecki bioregion. There is a weak negative correlation between the SOI and land erodibility in the Mulga Lands only. This is supported by the rainfall-erodibility relationship and a positive correlation ($r^2 = 0.56$, $p < 0.05$) between the PDO and land erodibility. There are weak correlations between land erodibility and the PDO in the Channel Country and Mitchell Grass Downs, but there is no correlation between the PDO and erodible land cover in the Simpson-Strzelecki Dune fields.

[35] Figures 6a and 6b present plots of mean annual rainfall, annual total erodible land cover and the Troup SOI for the four study area bioregions. We draw on this data to interpret mechanisms driving the temporal patterns and correlations between land erodibility, rainfall and climate indices (Table 1).

[36] In the Mulga Lands peaks in land erodibility coincide with negative SOI phases in 1982, 1986–1987, 1992–1994 and from 2002 to 2006 (Figure 6b). The peaks are consistent with those years receiving low annual rainfall (<300 mm). Reductions in erodible land in the remaining years are consistent with those years receiving annual rainfall >400 mm. Figure 6b shows evidence of a lag response in land erodibility change relative to shifts in the SOI phase. This is evident in the transition from the wet La Niña conditions from 1988 to 1990 to the dry El Niño event from 1991 to 1994 but is not present at every change. A mechanism behind the lag is the steady rather than rapid increase in annual rainfall from 1988 to 1990 (Figure 6a), and sustained vegetation cover over the bioregion until the drought in 1992. Short (~1 year) El Niño events, for example, in 1997, may not cause a reduction in rainfall.

Land erodibility may therefore continue to increase or decrease through these periods in line with trends determined by antecedent rainfall conditions.

[37] The Mitchell Grass Downs, Channel Country and Simpson-Strzelecki Desert bioregions appear to be more sensitive to intense and persistent (multiyear) drought than to interannual rainfall and ENSO variability (Table 1 and Figure 6b). This may explain the stronger positive correlations of land erodibility with the PDO in the Channel Country and Mitchell Grass Downs.

[38] The Mitchell Grass Downs experiences high inter-annual rainfall variability (Figure 6a); however, the rainfall is adequate to sustain regionally high vegetation cover levels and low land erodibility (Figure 6b). Peaks in land erodibility tend to occur in the northwestern half of the bioregion. This area, between Boulia and Urandangie, receives lower annual rainfall than the eastern half of the bioregion and is subsequently more sensitive to drought (e.g., 1986–1989). While rainfall has a strong association with El Niño events in the Mitchell Grass Downs [*McKeon et al.*, 2004], variability over the eastern half of the bioregion is not sufficient to induce regular regional scale (10^4 km²) changes in land erodibility that would provide strong correlations with either rainfall or the SOI.

[39] Land erodibility dynamics in the Channel Country reflect rainfall variability and the PDO more than ENSO phase changes (Table 1). The gradual increase in land erodibility between 1982 and 1988 (Figure 6b) is consistent with sustained "neutral" ENSO conditions and intensification of the PDO (cooling of sea surface temperatures in the tropical west Pacific). The bioregion received <200 mm annual rainfall in that period (Figure 6a). Subsequent peaks in land erodibility in 1994–1996 and 2004–2006 also follow extended (>4 year) periods of low rainfall. A lag response of land erodibility to rainfall is evident and short (1 year) periods of increased annual rainfall, for example, 200 mm in 1995, may not induce an immediate regional-scale decline in land erodibility.

[40] Land erodibility dynamics in the Simpson-Strzelecki Dune fields suggest that conditions in the bioregion may remain consistent for a number of years unless a significant change in local climate takes place. Changes in the area covered by moderate to highly erodible land occurred in the El Niño drought years of 1994–1996 and 2001–2006 (Figure 5). The second increase in highly erodible land only occurred following 6 years of annual rainfall <150 mm (Figure 6a). A reduction (down to <1% of the bioregion) in highly erodible land was only experienced from 1999 to 2000 following three successive years with annual rainfall >300 mm, and the net change in erodible land during this period was <10% (Figure 6b).

6. Discussion

6.1. Spatial Patterns in Land Erodibility

[41] The areas identified by AUSLEM as having high to moderate land erodibility match the spatial pattern of areas recording the highest dust storm frequencies in the northeastern half of the Lake Eyre Basin [*Middleton*, 1984; *Burgess et al.*, 1989; *McTainsh et al.*, 1990]. Dust storm frequencies decline to the east of Longreach and Charleville (Figure 1a) and the model assessments of land erodibility
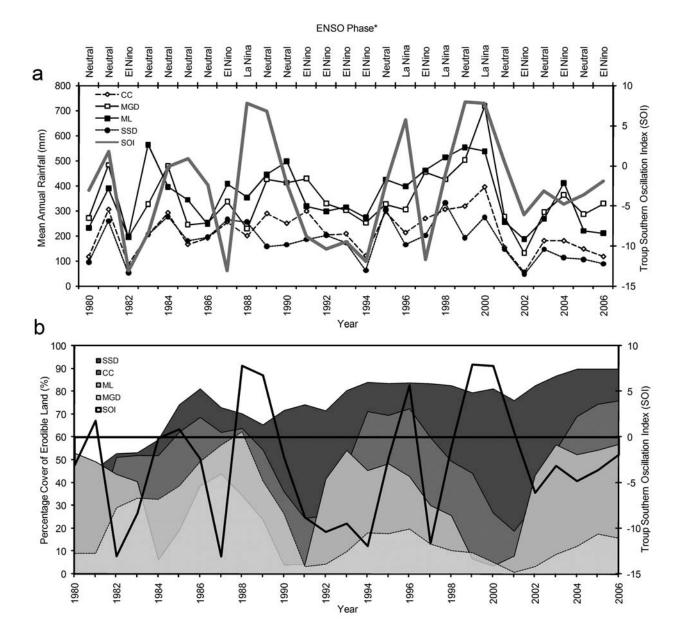
Figure 6. (a) Graphs mean annual rainfall and (b) percentage cover of erodible land with the Troup SOI for the four study area bioregions: Channel Country (CC); Mitchell Grass Downs (MGD); Mulga Lands (ML), and; Simpson-Strzelecki Dune fields (SSD). Years are classified into ENSO phases after *McKeon et al.* [2004].

are consistent with this pattern. *Miles and McTainsh* [1994] and *McTainsh et al.* [1999] reported high spatial variability in wind erosion activity in the Channel Country and Mulga Lands. This is reflected in the heterogeneity of land erodibility in these regions (Figure 2).

[42] The landforms associated with erodible land, e.g., river floodplains and dune fields, are consistent with those in other global dust source areas [*Washington et al.*, 2003]. AUSLEM assessments of low land erodibility over the Simpson Desert are not, however, consistent with records of wind erosion activity in that area [*McTainsh et al.*, 1990]. The assessments are contrary to the presence of the longitudinal dune fields that traverse the bioregion. This dune

field can become an active dust source area following the removal of vegetation by fire [*McGowan and Clark*, 2008].

[43] A number of factors affect model performance in the Simpson Desert. Subgrid scale averaging of vegetation cover over the model 5 × 5 km grid cells resulted in an inability to detect narrow (10–15 m) erodible dune crests that have an average spacing of ∼500 m [*Purdie*, 1984]. Furthermore, because the region is a National Park the Aussie GRASS plant consumption rates (by livestock) are kept low, resulting in consistently high cover predictions [*Carter et al.*, 1996]. Finally, fire burn scars were not delineated in the model input data. In November 2001 and January 2002 extensive burning of the Simpson Desert

resulted in the denudation of ~4000 km^2 (10%) of the bioregion. These events resulted in a proportional increase in the area of the bioregion susceptible to wind erosion, and the model has therefore underestimated the extent of erodible land between 2001 and 2006. These issues highlight the importance of data resolution and currency in the performance of spatially explicit wind erosion models. Updating the model inputs to account for fire burn scars and running the model at a higher spatial resolution, e.g., 30 m, would be required to improve model performance in the Simpson Desert bioregion.

6.2. Temporal Patterns in Land Erodibility

[44] Factors affecting temporal patterns in land erodibility include: climate, in particular rainfall quantities and distribution; land management practices, manifested here through stocking rates that affect the model grass cover inputs, and finally; the sensitivity of the bioregions to these external forcing mechanisms as governed by geomorphology, soil characteristics and vegetation structure and resilience.

[45] Results show that land erodibility in western Queensland is responsive to multiyear (>2 years) rainfall deficiencies (drought) and periods of above average rainfall. Similar responses have been reported in dust source areas in the African Sahel and North America [e.g., *Brooks and Legrand*, 2000; *Prospero and Lamb*, 2003; *Reheis*, 2006]. Significant increases in the areas of land susceptible to wind erosion occur in drought years (Figures 6a and 6b). The landscape response to drought varied between bioregions and is dependent on antecedent rainfall and vegetation conditions, which can generate lag responses in land erodibility change [also *Peters and Eve*, 1995]. The modeled increases in land erodibility with drought are consistent with reports of increased wind erosion activity over the study area [e.g., *McTainsh et al.*, 1989], and a global dependence of temporal variations in wind erosion on episodic droughts [*Middleton*, 1985; *Goudie and Middleton*, 1992; *Gao et al.*, 2003]. The length of the data time series (27 years) affected the correlations between land erodibility and the PDO, and so interpretations of the influence of interdecadal variations in the PDO should be treated with caution.

[46] The spatial extent of drought in western Queensland is dependent on the rainfall relationship with ENSO [*Crimp and Day*, 2003]. However, temporal patterns in areas affected by drought may vary considerably from year to year [*McKeon et al.*, 2004]. The poor correlation between modeled land erodibility and the SOI (Table 1) is a result of this phenomenon. Sustained negative SOI phases (El Niño) are associated with extended periods of warm sea surface temperatures (SST) in the equatorial eastern Pacific Ocean, a weakening of the Walker circulation and reduced convection over the Australian continent [*Troup*, 1965]. Positive SOI phases (La Niña) are associated with a strengthening of the Walker circulation and easterly trade winds and may result in enhanced convection and rainfall over parts of eastern Australia [*Sturman and Tapper*, 2001]. The association of peaks in land erodibility over the study area during El Niño driven drought events suggests that despite the poor correlation ENSO plays an important role in modulating land erodibility dynamics in western Queensland.

[47] ENSO-PDO interactions add complexity to understanding rainfall and drought variability in western Queens-

land. *Power et al.* [1999] reported on the interdecadal modulation of ENSO and its effects on rainfall in Australia. Their results showed that warm (positive) and cool (negative) phases of the PDO may enhance or suppress positive and negative SOI phases and the probability of eastern Australia receiving above or below average rainfall. *McKeon et al.* [2004] reported that less than 10% of years (1890–1991) with a combined negative SOI and cool PDO exceeded median annual rainfall in the Mulga Lands and Strzelecki Desert regions of southwest Queensland. Conversely, during positive SOI-cool PDO phases >70% of years in the analysis period received above average rainfall over the entire study area. For the period 1980 to 2006 the PDO was consistently in a warm phase. The impact of this on rainfall may have been in enhancing drought over the study area during El Niño events and increasing rainfall in the Mulga Lands during La Niña events [*McKeon et al.*, 2004]. The implications of this in terms of land erodibility change are difficult to surmise. Table 1 suggests that in the Mulga Lands at least, increases in land erodibility are related to periods of decreasing rainfall, negative SOI and warm PDO. The weaker correlation between rainfall and the SOI in southern and western Australia [*Pittock*, 1975] suggests that the relationship between land erodibility and ENSO will be weaker outside the current study area. Extending the length and coverage of the model simulation back to the 1950s would provide an opportunity to asses a larger combination of land erodibility, rainfall variability, ENSO and PDO conditions across Australia and would improve our ability to quantify the nature of their interactions in other bioregions.

[48] It is conceivable that additional climate oscillations will affect land erodibility in western Queensland. Such oscillations include the Madden Julian Oscillation (MJO) that has been shown to affect rainfall over northern Australia on a 30–60 day cycle [*Donald et al.*, 2006], and at interannual time scales teleconnections like the Indian Ocean Dipole (IOD) [*Saji et al.*, 1999]. The IOD has been shown to operate independently of ENSO with a 2 year periodicity [*Ashok et al.*, 2003a; *Behera and Yamagata*, 2003], and has been found to have a significant impact on rainfall in western and southern Australia [*Ashok et al.*, 2003b]. Globally, the significance of these and other teleconnections will vary considerably between continents [*Ginoux et al.*, 2004]. Determining the influence of teleconnections like the MJO and IOD on rainfall and land erodibility in western Queensland requires that their effects can be separated from those of ENSO and the PDO. Analysis of land erodibility-climate interactions at higher temporal resolutions, e.g., monthly, is necessary to achieve this but is beyond the capabilities of a model lacking a robust soil erodibility scheme [*Webb et al.*, 2009].

[49] Finally, the sensitivity of the bioregions to land erodibility change can be described. Results show that the Mulga Lands are most sensitive to climate variability. This is supported by the correlation of land erodibility with rainfall, the SOI and the PDO (Table 1), and historical reports of land degradation in the bioregion in response to drought and overgrazing in the 1960s, 1970s and early 1980s [*McKeon et al.*, 2004]. The sensitivity of the bioregion to degradation can be attributed to the region's arid climate, high stocking rates and the fragmented nature of the

landscape [*Stokes et al.*, 2008]. These factors contribute to low vegetation resilience to short-term climate variability and a response of significant reductions in understory grass cover during periods of low rainfall. This sensitivity exists in other similarly fragmented semiarid rangelands around the world [*Galvin et al.*, 2008], suggesting that other dust source areas will be as responsive to global teleconnections.

[50] Land erodibility changes in the Channel Country may occur at a similar time scales as in Mulga Lands. However, rapid (<1 year) increases in high-erodibility land do not occur as frequently. At the regional scale, the Mitchell Grass Downs and Simpson-Strzelecki bioregions have relatively lower sensitivities to interannual rainfall variability. This is indicated by the low net fluctuations in erodible land over the bioregions for much of the period from 1980 to 2006. These bioregions are sensitive to high-magnitude changes in regional climate affecting rainfall. In the Mitchell Grass Downs this sensitivity is indicated by widespread elevations in erodibility during intense droughts (up to 60% of the bioregion), and the near complete reduction in erodible land cover (to <20%) between 1990 and 2006. In the Simpson-Strzelecki bioregion this sensitivity is indicated by a reduction (to <1%) in highly erodible land under the regionally wet 1998 and 2000 La Niña events. A genetic ability of the dominant Spinifex vegetation (*Triodia* spp.) to survive under an arid climate contributes to the low net variation in the erodibility in the Simpson Desert except under extreme environmental change [*Specht and Specht*, 1999].

[51] Regional-scale field surveys to monitor temporal changes in the susceptibility of these bioregions to wind erosion and extended (>30 years) simulations of land erodibility are required to elucidate more specific characteristics of the sensitivity of western Queensland to climate variability and management.

7. Conclusions

[52] This research has examined spatial and temporal patterns in land erodibility in western Queensland, Australia. Results show that the Strzelecki dune fields and outer floodplains of the Channel Country river systems were consistently susceptible to wind erosion from 1980 to 2006. These spatial patterns in land erodibility indentified by AUSLEM are consistent with observational records of wind erosion activity within the study area. Mean seasonal variations in land erodibility across western Queensland are weak and driven by rainfall seasonality. Conversely, variations at interannual time scales can be large, with regional-scale land erodibility dynamics being influenced by antecedent climatic conditions and the landscape sensitivity to rainfall, ENSO and PDO interactions. These drivers can result in complex lag responses in land erodibility change. In a global context the research has highlighted the dynamic nature of land erodibility, and the importance mapping and monitoring land erodibility to improve our understanding of the effects of land management and future climatic changes on wind erosion processes.

[53] Further research into land erodibility dynamics in Australia requires an extension of that presented here. First, research should focus on extending the length of the model simulations. This would allow variations in land erodibility

to be analyzed under a greater range of ENSO and PDO conditions. Second, effort should be directed toward developing schemes to simulate temporal changes in soil erodibility in rangeland environments. Land erodibility dynamics over small (subregional) spatial and monthly temporal scales are highly dependent on soil erodibility, particularly in landscapes with sparse vegetation cover. The addition of a robust soil erodibility scheme to AUSLEM would improve model skill in assessing land erodibility. It would also allow for analyses of model output at higher temporal resolutions and an ability to assess the impacts of short- and long-term land management practices on potential wind erosion activity. Finally, analyses should be extended to include the southern and western regions of Australia over both rangelands and cultivated environments as these regions are likely to experience significant change in response to future climate change [*Meehl et al.*, 2007].

References

Allan, R. J. (1988), El Niño–Southern Oscillation influences in the Australasian region, *Prog. Phys. Geogr.*, *12*, 313–348, doi:10.1177/030913338801200301.

Ashok, K., Z. Guan, and T. Yamagata (2003a), A look at the relationship between the ENSO and the Indian Ocean Dipole, *J. Meteorol. Soc. Jpn.*, *81*, 41–56, doi:10.2151/jmsj.81.41.

Ashok, K., Z. Guan, and T. Yamagata (2003b), Influence of the Indian Ocean dipole on the Australian winter rainfall, *Geophys. Res. Lett.*, *30*(15), 1821, doi:10.1029/2003GL017926.

Behera, S. K., and T. Yamagata (2003), Influence of the Indian Ocean dipole on the Southern Oscillation, *J. Meteorol. Soc. Jpn.*, *81*, 169–177, doi:10.2151/jmsj.81.169.

Brooks, N., and M. Legrand (2000), Dust variability and rainfall in the Sahel, in *Linking Climate Change to Land-Surface Change*, edited by S. McLaren and D. Kniveton, pp. 1–25, Kluwer Acad., Dordrecht, Netherlands.

Bullard, J. E., M. C. Baddock, G. H. McTainsh, and J. F. Leys (2008), Sub-basin scale dust source geomorphology detected using MODIS, *Geophys. Res. Lett.*, *35*, L15404, doi:10.1029/2008GL033928.

Burgess, R. C., G. H. McTainsh, and J. R. Pitblado (1989), An index of wind erosion in Australia, *Aust. Geogr. Stud.*, *27*, 98–110, doi:10.1111/j.1467-8470.1989.tb00594.x.

Carter, J. O., N. Flood, G. McKeon, A. Peacock, and A. Beswick (1996), Development of a national drought alert strategic information system: Model framework, parameter derivation, model calibration, model validation, model outputs, Web technology, Final Report on QPI 20 to Land and Water Resources Research and Development Corporation, *Rep. LWRRDC QPI 20*, Dep. of Nat. Resour., Indooroopilly, Queensl., Australia.

Crimp, S. J., and K. A. Day (2003), Evaluation of multi-decadal variability in rainfall in Queensland using indices of El Niño–Southern Oscillation and inter-decadal variability, in *National Drought Forum 2003: Science for Drought*, pp. 106–115, Commonw. Bur. of Meteorol., Melbourne.

Danaher, T. J., J. D. Armston, and L. J. Collett (2004), A multiple regression model for the estimation of woody foliage cover using Landsat in Queensland, Australia, paper presented at the International Geoscience and Remote Sensing Symposium (IGARSS), NASA Earth Sci. Enterprise, Data and Serv., Land Process. Distributed Act. Arch. Cent., Anchorage, Alaska.

Donald, A., H. Meinke, B. Power, A. de H. N. Maia, M. C. Wheeler, N. White, R. C. Stone, and J. Ribbe (2006), Near-global impact of the Madden-Julian Oscillation on rainfall, *Geophys. Res. Lett.*, *33*, L09704, doi:10.1029/2005GL025155.

Ekström, M., G. H. McTainsh, and A. Chappell (2004), Australian dust storms: Temporal trends and relationships with the synoptic pressure distributions during 1960–99, *Int. J. Climatol.*, *24*, 1581–1599, doi:10.1002/joc.1072.

Findlater, P. A., D. J. Carter, and W. D. Scott (1990), A model to predict the effects of prostrate ground cover on wind erosion, *Aust. J. Soil Res.*, 28, 609–622, doi:10.1071/SR9900609.

Fryrear, D. W. (1985), Soil cover and wind erosion, *Trans. ASAE*, 28(3), 781–784.

Galvin, K. A., R. S. Reid, R. H. Behnke Jr., and N. Thompson Hobbs (Eds.) (2008), *Fragmentation in Semi-arid and Arid Landscapes: Consequences for Human and Natural Systems*, 411 pp., Springer, Dordrecht, Netherlands.

Gao, T., L. Su, Q. Ma, H. Li, X. Li, and X. Yu (2003), Climatic analyses on increasing dust storm frequency in the springs of 2000 and 2001 in Inner Mongolia, *Int. J. Climatol.*, 23, 1743–1755, doi:10.1002/joc.970.

Gillette, D. A. (1999), A qualitative geophysical explanation for "Hot Spot" dust emitting source regions, *Contrib. Atmos. Phys.*, 72, 67–77.

Ginoux, P., M. Chin, I. Tegen, J. M. Prospero, B. Holben, O. Dubovik, and S.-J. Lin (2001), Sources and distributions of dust aerosols simulated with the GOCART model, *J. Geophys. Res.*, 106, 20,255–20,273, doi:10.1029/2000JD000053.

Ginoux, P., J. M. Prospero, O. Torres, and M. Chin (2004), Long-term simulation of global dust distribution with the GOCART model: Correlation with North Atlantic Oscillation, *Environ. Model. Software*, 19, 113–128, doi:10.1016/S1364-8152(03)00114-2.

Goudie, A. S., and N. J. Middleton (1992), The changing frequency of dust storms through time, *Clim. Change*, 20, 197–225, doi:10.1007/BF00139839.

Goudie, A. S., and N. J. Middleton (2006), *Desert Dust in the Global System*, 287 pp., Springer, Berlin, Germany.

Grini, A., G. Myhre, C. S. Zender, and I. S. A. Isaksen (2005), Model simulations of dust sources and transport in the global atmosphere: Effects of soil erodibility and wind speed variability, *J. Geophys. Res.*, 110, D02205, doi:10.1029/2004JD005037.

Hara, Y., I. Uno, and Z. Wang (2006), Long-term variation of Asian dust and related climate factors, *Atmos. Environ.*, 40, 6730–6740, doi:10.1016/j.atmosenv.2006.05.080.

Hassett, R. C., H. L. Wood, J. O. Carter, and T. J. Danaher (2000), A field method for statewide ground-truthing of a spatial pasture growth model, *Aust. J. Exp. Agric.*, 40, 1069–1079, doi:10.1071/EA00010.

Hu, Y., and Q. Fu (2007), Observed poleward expansion of the Hadley circulation since 1979, *Atmos. Chem. Phys.*, 7, 5229–5236.

Jickells, T. D., et al. (2005), Global iron connections between desert dust, ocean biogeochemistry, and climate, *Science*, 308, 67–71, doi:10.1126/science.1105959.

Lal, R. (2001), Soil degradation by erosion, *Land Degrad. Rehabil.*, 12, 519–539, doi:10.1002/ldr.472.

Leys, J. F. (1991), Towards a better model of the effect of prostrate vegetation cover on wind erosion, *Vegetatio*, 91, 49–58, doi:10.1007/BF00036047.

Littleboy, M., and G. M. McKeon (1997), Final report for the Rural Industries Research and Development Corporation, Appendix 2, Subroutine GRASP: Grass Production Model, Climate Impacts and Applications, Dep. of Nat. Resour., Indooroopilly, Queensl., Australia.

Lu, H., and Y. Shao (2001), Toward quantitative prediction of dust storms: An integrated wind erosion modeling system and its applications, *Environ. Model. Software*, 16, 233–249, doi:10.1016/S1364-8152(00)00083-9.

Lyles, L., and B. E. Allison (1981), Equivalent wind erosion protection from selected crop residues, *Trans. ASAE*, 24, 405–408.

Mahowald, N. M., R. G. Bryant, J. del Corral, and L. Steinberger (2003a), Ephemeral lakes and desert dust sources, *Geophys. Res. Lett.*, 30(2), 1074, doi:10.1029/2002GL016041.

Mahowald, N. M., C. Luo, and J. del Corral (2003b), Interannual variability in atmospheric mineral aerosols from a 22-year model simulation and observational data, *J. Geophys. Res.*, 108(D12), 4352, doi:10.1029/2002JD002821.

Mantua, N. J., S. R. Hare, Y. Zhang, J. M. Wallace, and R. C. Fracis (1997), A Pacific interdecadal climate oscillation with impacts on salmon production, *Bull. Am. Meteorol. Soc.*, 78, 1069–1079, doi:10.1175/1520-0477(1997)078<1069:APICOW>2.0.CO;2.

Marshall, J. K. (1972), Principles of soil erosion and its prevention, in *The Use of Trees and Shrubs in the Dry Country of Australia*, pp. 90–107, Dep. of Natl. Dev., For. and Timber Bur. Aust. Govt. Pub. Serv., Canberra.

Marticorena, B., and G. Bergametti (1995), Modeling the atmospheric dust cycle: 1. Design of a soil-derived dust emission scheme, *J. Geophys. Res.*, 100, 16,415–16,416, 430, doi:10.1029/95JD00690.

McBride, J. L, and N. Nicholls (1983), Seasonal relationships between Australian rainfall and the Southern Oscillation, *Mon. Weather Rev.*, 111, 1998–2004, doi:10.1175/1520-0493(1983)111<1998:SRBARA>2.0.CO;2.

McGowan, H. A., and A. Clark (2008), A vertical profile of PM10 dust concentrations measured during a regional dust event identified by MODIS Terra, western Queensland, Australia, *J. Geophys. Res.*, 113, F02S03, doi:10.1029/2007JF000765.

McKeon, G. M., W. B. Hall, B. K. Henry, G. S. Stone, and I. W. Watson (Eds.) (2004), *Pasture Degradation and Recovery in Australias Rangelands: Learning From History*, 256 pp., Queensl. Dep. of Nat. Resour., Mines and Energy, Brisbane.

McTainsh, G. H., and J. F. Leys (1993), Soil Erosion by Wind, in *Land Degradation Processes in Australia*, edited by G. H. McTainsh and W. C. Boughton, pp. 188–233, Longman-Cheshire, Melbourne, Queensl., Australia.

McTainsh, G. H., R. Burgess, and J. R. Pitblado (1989), Aridity, drought and dust storms in Australia (1960–84), *J. Arid Environ.*, 16, 11–22.

McTainsh, G. H., A. W. Lynch, and R. Burgess (1990), Wind erosion in eastern Australia, *Aust. J. Soil Res.*, 28, 323–339, doi:10.1071/SR9900323.

McTainsh, G. H., A. W. Lynch, and E. K. Tews (1998), Climatic controls upon dust storm occurrence in eastern Australia, *J. Arid Environ.*, 39, 457–466, doi:10.1006/jare.1997.0373.

McTainsh, G. H., J. F. Leys, and W. G. Nickling (1999), Wind erodibility of arid lands in the channel country of western Queensland, Australia, *Z. Geomorphol.*, 116, 113–130.

Meehl, G. A., et al. (2007), Global climate projections, in *Climate Change 2007: The Physical Science Basis: Contribution of Working Group I to the Fourth Assessment Report of the Intergovernmental Panel on Climate Change*, pp. 747–845, Cambridge Univ. Press, Cambridge, U.K.

Middleton, N. J. (1984), Dust storms in Australia: Frequency, distribution and seasonality, *Search*, 15, 46–47.

Middleton, N. J. (1985), Effect of drought on dust production in the Sahel, *Nature*, 316, 431–434, doi:10.1038/316431a0.

Miles, R., and G. H. McTainsh (1994), Wind erosion and land management in the mulga lands of Queensland, *Aust. J. Soil Water Conserv.*, 7, 41–45.

Miller, R. L., and I. Tegen (1998), Climate response to soil dust aerosols, *J. Clim.*, 11, 3247–3267, doi:10.1175/1520-0442(1998)011<3247:CRTSDA>2.0.CO;2.

Moulin, C., C. E. Lambert, F. Dulac, and U. Dayan (1997), Control of atmospheric export of dust from North Africa by the North Atlantic Oscillation, *Nature*, 387, 691–694, doi:10.1038/42679.

Okin, G. S., and M. C. Reheis (2002), An ENSO predictor of wind erosion and dust emission in the southwest United States, *Geophys. Res. Lett.*, 29(9), 1332, doi:10.1029/2001GL014494.

Oldeman, L. R. (1994), The global extent of soil degradation, in *Soil Resilience and Sustainable Land Use: Proceedings of a symposium held in Budapest, 28 September to 2 October 1992, including the Second Workshop on the Ecological Foundations of Sustainable Agriculture (WEFSA II)*, edited by D. J. Greenland and I. Szabolcs, pp. 99–118, CAB Int., Wallingford, U.K.

Peters, A. J., and M. D. Eve (1995), Satellite monitoring of desert plant community response to moisture availability, *Environ. Monit. Assess.*, 37, 273–287, doi:10.1007/BF00546895.

Pittock, A. B. (1975), Climatic change and the patterns of variation in Australian rainfall, *Search*, 6, 498–504.

Power, S., T. Casey, C. Folland, A. Colman, and V. Mehta (1999), Interdecadal modulation of the impact of ENSO on Australia, *Clim. Dyn.*, 15, 319–324, doi:10.1007/s003820050284.

Prospero, J. M., and P. J. Lamb (2003), African droughts and dust transport to the Caribbean: Climate change implications, *Science*, 302, 1024–1027, doi:10.1126/science.1089915.

Prospero, J. M., P. Ginoux, O. Torres, S. E. Nicholson, and T. E. Gill (2002), Environmental characterization of global sources of atmospheric soil dust identified with the NIMBUS 7 Total Ozone Mapping Spectrometer (TOMS) absorbing aerosol product, *Rev. Geophys.*, 40(1), 1002, doi:10.1029/2000RG000095.

Purdie, R. (1984), *Land Systems of the Simpson Desert Region, CSIRO Division of Land Resources, Natural Resources Series No. 2*, CSIRO, Melbourne.

Queensland Department of Primary Industries (QDPI) (1974), Western Arid Regions Land Use Study (WARLUS), *Tech. Bull. 12*, Div. of Land Utilisation, Brisbane.

Reheis, M. C. (2006), A 16-year record of eolian dust in Southern Nevada and California, USA: Controls on dust generation and accumulation, *J. Arid Environ.*, 67, 487–520, doi:10.1016/j.jaridenv.2006.03.006.

Saji, N. H., B. N. Goswami, P. N. Vinayachandran, and T. Yamataga (1999), A dipole mode in the tropical Indian Ocean, *Nature*, 401, 360–363.

Shao, Y. (2000), *Physics and Modelling of Wind Erosion*, 393 pp., Kluwer Acad., London.

Shao, Y., and L. M. Leslie (1997), Wind erosion prediction over the Australian continent, *J. Geophys. Res.*, 102, 30,091–30,105.

Shao, Y., M. R. Raupach, and J. F. Leys (1996), A model for predicting aeolian sand drift and dust entrainment on scales from paddock to region, *Aust. J. Soil Res.*, 34, 309–342, doi:10.1071/SR9960309.

Shao, Y., J. F. Leys, G. H. McTainsh, and K. Tews (2007), Numerical simulation of the October 2002 dust event in Australia, *J. Geophys. Res.*, *112*, D08207, doi:10.1029/2006JD007767.

Sivakumar, M. V. K. (2007), Interactions between climate and desertification, *Agric. For. Meteorol.*, *142*, 143–155, doi:10.1016/j.agrformet. 2006.03.025.

Specht, R. L., and A. Specht (1999), *Australian plant communities: Dynamics of structure, growth and biodiversity*, 492 pp., Oxford Univ. Press, Melbourne.

Stokes, C. J., R. R. J. McAllister, A. J. Ash, and J. E. Gross (2008), Changing Patterns of Land Use and Tenure in the Dalrymple Shire, Australia, in *Fragmentation in Semi-arid and Arid Landscapes: Consequences for Human and Natural Systems*, edited by K. A. Galvin et al., pp. 93–112, Springer, Dordrecht, Netherlands.

Sturman, A., and N. Tapper (2001), *The Weather and Climate of Australia and New Zealand*, 476 pp., Oxford Univ. Press, Melbourne.

Troup, A. J. (1965), The Southern Oscillation, *Q. J. R. Meteorol. Soc.*, *91*, 490–506, doi:10.1002/qj.49709139009.

Washington, R., M. Todd, N. J. Middleton, and A. S. Goudie (2003), Dust-storm source areas determined by the Total Ozone Monitoring Spectrometer and surface observations, *Ann. Assoc. Am. Geogr.*, *93*, 297–313, doi:10.1111/1467-8306.9302003.

Webb, N. P., H. A. McGowan, S. R. Phinn, and G. H. McTainsh (2006), AUSLEM (Australian Land Erodibility Model): A tool for identifying wind erosion hazard in Australia, *Geomorphology*, *78*, 179–200, doi:10.1016/j.geomorph.2006.01.012.

Webb, N. P., H. A. McGowan, S. R. Phinn, G. H. McTainsh, and J. F. Leys (2009), A model to predict land susceptibility to wind erosion in western Queensland, Australia, *Environ. Model. Software*, *24*, 214–227, doi:10.1016/j.envsoft.2008.06.006.

Zender, C. S., and E. Y. Kwon (2005), Regional contrasts in dust emission responses to climate, *J. Geophys. Res.*, *110*, D13201, doi:10.1029/2004JD005501.

Zender, C. S., H. Bian, and D. Newman (2003a), The mineral Dust Entrainment and Deposition (DEAD) model: Description and 1990s dust climatology, *J. Geophys. Res.*, *108*(D14), 4416, doi:10.1029/2002JD002775.

Zender, C. S., D. Newman, and O. Torres (2003b), Spatial heterogeneity in aeolian erodibility: Uniform, topographic, geomorphic, and hydrologic hypotheses, *J. Geophys. Res.*, *108*(D17), 4543, doi:10.1029/2002JD003039.

———————————
J. F. Leys, Scientific Services Division, Department of Environment and Climate Change, New South Wales Government, P.O. Box 462, 9127 Kamilaroi Highway, Gunnedah, NSW 2380, Australia.

H. A. McGowan, School of Geography, Planning and Architecture, University of Queensland St. Lucia, Brisbane, Qld 4072, Australia.

G. H. McTainsh, Australian Rivers Institute, Faculty of Environmental Sciences, Griffith University, Brisbane, Qld 4111, Australia.

S. R. Phinn and N. Webb, Centre for Remote Sensing and Spatial Information Science, School of Geography, Planning and Architecture, University of Queensland St. Lucia, Brisbane, Qld 4072, Australia. (nick.webb01@gmail.com)